Feedback stabilization of unstable propagating waves

Eugene Mihaliuk,[1] Tatsunari Sakurai,[1] Florin Chirila,[1] and Kenneth Showalter[1,2]
[1]*Department of Chemistry, West Virginia University, Morgantown, West Virginia 26506*
[2]*Fritz-Haber-Institut der Max-Planck-Gesellschaft, Faradayweg 4-6, 14195 Berlin, Germany*

Propagating wave segments are stabilized to a constant size and shape by applying negative feedback from the measured wave area to the excitability of the medium. The locus of steady-state wave size as a function of excitability defines the perturbation threshold for the initiation of spiral waves. This locus also defines the excitability boundary for spiral wave behavior in active media.

Propagating waves in active media arise from the coupling of a positive feedback process, such as chemical autocatalysis, with some form of mass transport, such as molecular diffusion. A variety of spatiotemporal patterns arise from the interplay of these processes, from expanding circular and spiral waves [1–3] to highly disordered structures that resemble turbulence [4–6]. Completely new types of spatiotemporal behavior, such as traveling spots [7], spiral wave resonance attractors [8], and oscillatory clusters [9] arise in reaction-diffusion systems that include elements of global feedback.

The basic features of wave propagation are largely determined by the excitability of the medium, and two excitability limits can be identified for 1D and 2D wave propagation [10]. The propagation of 1D waves is not possible below one excitability limit, and 2D waves with free ends, such as spiral waves or wave segments, contract and disappear below the other excitability limit.

In this paper, we present a detailed characterization of the excitability limit for 2D waves with free ends. The evolution of such waves is influenced not only by the medium excitability but also by the wave size. At each excitability, there is a wave segment with a particular and natural form (length and shape) that will either grow or decay when perturbed. Wave segments larger than this critical wave form grow to fill the medium with spiral waves, while smaller wave segments contract until they disappear. The critical wave size increases with decreasing excitability, and the locus of this size as a function of excitability represents a perturbation threshold, separating an attractor characterized by spiral waves from an attractor characterized by the uniform steady state.

We study the locus of critical wave size by stabilizing unstable wave segments in the Belousov-Zhabotinsky (BZ) reaction with a feedback control algorithm. Waves are stabilized by continually adjusting the excitability of the medium such that it is decreased when the wave area increases and vice versa. We describe experimental and numerical studies of wave segment stabilization and also present a kinematic analysis.

Experiments were carried out with the photosensitive Belousov-Zhabotinsky (BZ) reaction [11,12] using a 0.3 mm×20 mm×30 mm slab of silica gel in which ruthenium(II)-bipyridyl, a light-sensitive catalyst for the BZ reaction, was immobilized. Images of chemical waves were captured with a video camera and processed by a computer in real time to modulate the beam intensity of a video projector illuminating the gel, thereby producing the desired medium excitability. Details of the experimental setup and the excitable medium preparation are described in [13].

Wave stabilization is realized by adjusting the light intensity ϕ incident on the gel according to the negative feedback algorithm

$$\phi = aA + b, \tag{1}$$

with area A and the feedback coefficient a and offset b. The area of the wave, corresponding to the region containing the oxidized ruthenium catalyst, $Ru(bpy)_3^{3+}$, is determined as the pixel count above a threshold:

$$A = \sum_{x,y} \Theta(p(x,y) - k \cdot \overline{p(x,y)}). \tag{2}$$

Here, $\Theta(\ )$ is the Heaviside function, $p(x,y)$ is the gray level at each pixel, and the threshold is a value slightly above the average gray level $\overline{p(x,y)}$ over the image ($k = 1.1$). This adaptive threshold scheme allows the wave area to be accurately determined in the presence of unavoidable light intensity fluctuations.

The excitability of the medium is reduced or increased as the wave becomes larger or smaller, respectively, according to the feedback algorithm. As the wave approaches its stationary size and shape the control perturbations become vanishingly small, with the stabilized state representing an intrinsic unstable state of the autonomous system (without control). Examples of the stabilized waves are shown in Fig. 1. Changing the offset b in the feedback loop results in different medium excitabilities and, hence, different wave sizes.

The essential features of the photosensitive BZ system are described by a two-variable Oregonator model [14,15] that has been modified to include the photochemical pathway [16]:

$$\frac{\partial u}{\partial t} = \frac{1}{\varepsilon} \left(u - u^2 - (fv + \phi) \frac{u - q}{u + q} \right) + D_u \nabla^2 u,$$
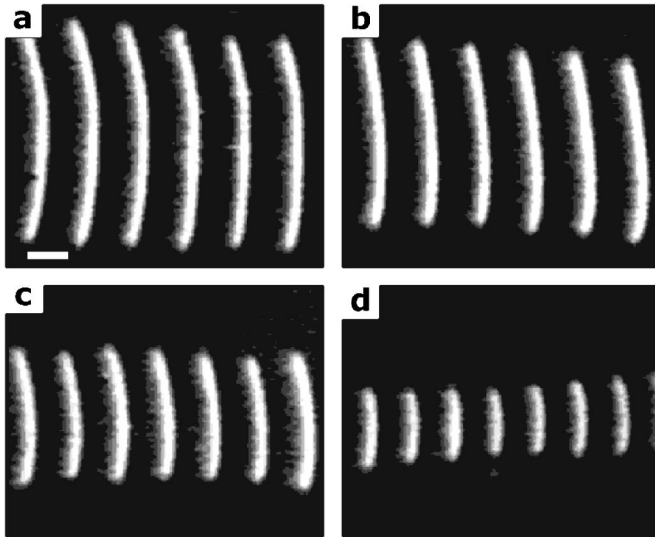
$$\frac{\partial v}{\partial t} = (u - v), \tag{3}$$

FIG. 1. Examples of typical wave segments stabilized by the feedback algorithm. The image in each panel represents an overlay of snapshots taken every 40.0 s. The feedback parameter a is 0.375 in all experiments. The values of the offset parameter b and resulting values of ϕ are -0.0744, 0.564 (a), -0.0248, 0.551 (b), 0.0248, 0.528 (c), and 0.0744, 0.488 (d), all measured in mW/cm^2. Composition of catalyst-free BZ solution: 0.28 M NaBrO$_3$, 0.05 M malonic acid, 0.165 M bromomalonic acid, 0.36 M H$_2$SO$_4$. Silica gel prepared by acidifying aqueous solution of 10% (w/w) Na$_2$SiO$_3$ and 2.0×10^{-3} M Ru(bpy)$_3^{2+}$ with H$_2$SO$_4$. Solution and gel were maintained at 9.0 °C. The scale bar in (a) is 1.0 mm and one pixel corresponds to 73 μm.

where the variables u and v correspond to HBrO$_2$ and Ru(bpy)$_3^{3+}$ concentrations, respectively, and D_u is the activator diffusion coefficient. The parameter ϕ, corresponding to the light intensity, controls the excitability of the medium. The kinetic parameters ϵ, q, and f are fixed at values such that the medium is excitable but nonoscillatory at $\phi=0$ and can be made nonexcitable by increasing ϕ.

The initial conditions in each calculation consist of a small wave segment that assumes a certain constant steady-state size and shape as the control algorithm is applied, as shown in Fig. 2(a). In the absence of control, the wave either contracts and eventually disappears or grows until it reaches the boundaries of the medium, as shown in panels (b) and (c). In this calculation, small perturbations were applied to accelerate the departure from the unstable steady state; however, an infinitesimal random perturbation would ultimately cause the unstable wave to grow or decay.

The steady-state wave area S increases with decreasing excitability, as shown in Fig. 3, with the area diverging at the critical value of the light intensity $\phi_{2\,\mathrm{D}}$. Different steady-state wave sizes on this curve can be selected and stabilized by changing the offset term b in the control loop. The circles show the results of the PDE simulations using Eqs. (3), and the solid curve shows the prediction from the kinematic analysis we now describe.

We consider a wave of constant size and shape propagating through a medium of a particular excitability. We will derive expressions describing the contour of such a wave and
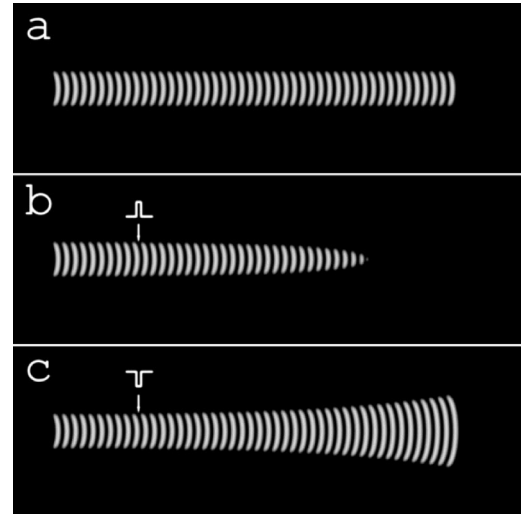

FIG. 2. Simulation of wave segment stabilization using Eqs. (3). Panel (a) shows the evolution of the wave segment under feedback control with the parameters $a=2.5\times10^{-4}$, $b=-0.14$, giving $\phi\approx0.0909$. In panels (b) and (c), the control was discontinued and a small perturbation of duration $\Delta t=0.1$ and amplitude $\Delta\phi=\pm1.0\times10^{-3}$ was applied, after which the light intensity was held at the value prior to the perturbation. Equations (3) were integrated using an Euler method with a time step of 5.0×10^{-4} and a grid size of 0.02 on an array of 1000×500 grid points with zero-flux boundary conditions. Parameter values: $\epsilon=0.01$, $f=2.5$, $q=0.002$, and $D_u=0.1$. The image in each panel represents an overlay of snapshots taken every 0.25 time units.

the dependence of the wave size on the excitability of the medium. Since the front is symmetrical, we consider the curve s representing one-half of the leading wave front, as shown in Fig. 4, with l being the coordinate along the curve. The origin of s at $y=0$ moves with the wave at velocity v_0 in the positive x direction. At any given point on the curve,
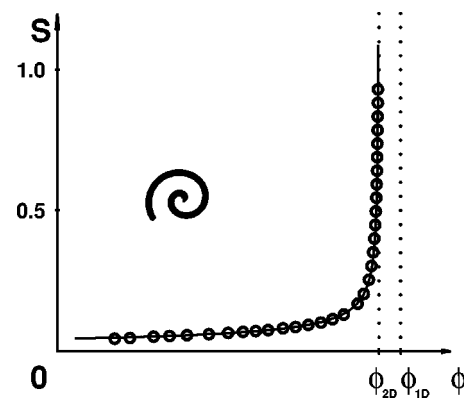

FIG. 3. Dependence of critical wave size S on light intensity ϕ. Values calculated with Eqs. (3) shown by circles. At $\phi_{2D}=0.0915$ the wave size diverges to infinity. The dark system with $\phi=0$, corresponding to the nonoscillatory but excitable experimental system, lies just above the Hopf bifurcation. The limit $\phi_{1D}=0.0977$ marks the point beyond which no propagation is possible for 1D waves. Model parameters and numerical integration are the same as in Fig. 2. Solid line shows prediction of kinematic model according to Eq. (11), where $c=4.15\times10^{-4}$, $D=0.16$, and $v_0=1.84$.
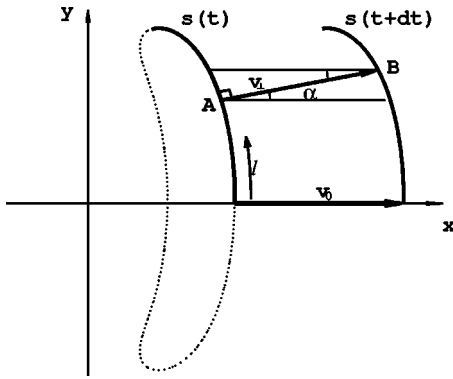
FIG. 4. One-half of the leading front of a wave segment propagating with velocity v_0 in the x direction. The angle between the normal direction to the front and the x direction is α, and $v_\perp$ is the normal velocity. Shape stationarity requires that every point A at time t becomes some point B at time $t+dt$ by propagation normal to the front. Dotted curve represents wave contour from the PDE simulations with the parameters as in Fig. 2. The thick curve corresponds to the half-front shape predicted from the kinematic description Eq. (7), where $K_0=0.42$, $D=0.16$, $v_0=1.84$, and l is the coordinate along the curve.

the normal to the front makes an angle α with the x direction, and α becomes $\pi/2$ at the extremum of the curve.

Now consider the wave front at two moments t and $t+dt$. To maintain shape stationarity, every point A of the curve $s(t)$ must become some point B of its rigidly translated replica $s(t+dt)$ by moving in the normal direction with velocity $v_\perp$. This geometric constraint can be written as

$$v_\perp = v_0 \cos(\alpha). \tag{4}$$

This stationarity condition provides a direct connection between $v_\perp$ as a function of curvature, $v_\perp = f(K)$, and the stationary wave shape $\alpha(l)$. We find a linear relationship between the curvature $\alpha(l)'$ and $\cos(\alpha) \propto v_\perp$ from contour lines obtained in numerical simulations and therefore employ a linear eikonal equation to describe the dependence of the normal velocity upon curvature:

$$v_\perp = v_\infty - DK, \tag{5}$$

where v_∞ is the velocity of the planar front, $K=\alpha'$ is the curvature, and D is a coefficient associated with the autocatalyst diffusivity [17]. Combining Eqs. (4) with (5), and expressing v_∞ in terms of K_0 and v_0, we obtain

$$v_0 \cos(\alpha) = v_0 + DK_0 - D\alpha', \tag{6}$$

where K_0 is the curvature at the midpoint of the wave.

For all but the smallest waves, most of the front corresponds to small values of α, and the solution of Eq. (6) is therefore well approximated by

$$\alpha = \lambda K_0 \tan(l/\lambda), \tag{7}$$

where
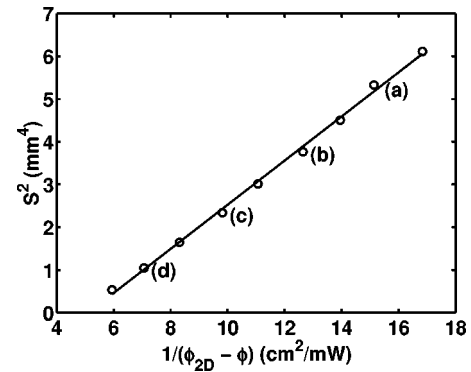

FIG. 5. Square of the wave size S^2 from experimental measurements as a function of inverse difference between ϕ and $\phi_{2D} = 0.63$ mW/cm^2. Points (a)–(d) correspond to the panels in Fig. 1. Experimental conditions and procedures are the same as in Fig. 1.

$$\lambda = \sqrt{\frac{2D}{v_0 K_0}}. \tag{8}$$

At the end point, $\alpha = \pi/2$, and, typically, $v_0 \gg DK_0$; therefore, the length L is

$$L \approx \frac{\pi\lambda}{2}, \tag{9}$$

since $\arctan(x) \approx \pi/2$ for $x \gg 1$. Based on measurements of curvature as a function of excitability in the PDE simulations, we approximate the dependence of K_0 on ϕ with the linear function

$$K_0 = (\phi_{2D} - \phi)/c, \tag{10}$$

where c is an empirical constant. Substituting relation (10) into Eq. (9) yields

$$L^2 \propto \frac{\pi^2 D}{2v_0} \frac{c}{(\phi_{2D} - \phi)}. \tag{11}$$

Here we neglect the dependence of D and v_0 on ϕ, which is small compared to that of K_0. A comparison of the kinematic description with the PDE simulations can be seen in Fig. 3, where the solid curve shows values of L from Eq. (11). (We note that S and L are proportional except for the smallest wave segments.)

Extensive theoretical studies have been carried out on spiral wave dynamics [18–22], and the excitability limit for spiral wave behavior has been described [10]. The wavelength of a spiral wave increases with decreasing excitability until it becomes infinite at the excitability limit. At this critical point, the unbounded spiral wave has completely opened up to form an unbounded planar wave with a free end. As the excitability is further decreased, the planar wave contracts at its free end. The excitability limit is defined as the point where the wave becomes planar and is stationary in the moving-coordinate system [10]. This excitability limit is exactly the same as the limit defined by the divergence of the steady-state wave segments at ϕ_{2D} in Fig. 3 [23]. The excitability where the steady-state wave segment becomes un-

bounded defines a critical point for two-dimensional media: at lower excitabilities, the asymptotic propagation of waves with free ends is not supported.

The kinematic description for propagating wave segments is in excellent agreement with the numerical simulations, as shown in Figs. 3 and 4. We note, however, that the good agreement for very short waves is likely fortuitous, as our assumptions above that depend on slight curvature are not applicable for these waves. The general agreement between the theoretical and simulated prediction of critical wave size S as a function of light intensity ϕ in Fig. 3 is due to the curvature contribution of the tip being negligible except for very small wave segments. We also note that the experimental measurements are in good agreement with the theoretical description, although only a relatively narrow range of excitability could be studied in our experiments. The size S of the experimental waves increases with increasing light intensity (decreasing excitability), as shown in Fig. 1. A linear dependence of S^2 on the inverse difference between ϕ and ϕ_{2D} is shown in Fig. 5, in agreement with the prediction of Eq. (11) from the kinematic description.

The feedback stabilization of unstable wave segments yields a characteristic curve of wave size as a function of excitability, the asymptote of which is the excitability limit for spiral wave behavior. This curve also represents a perturbation threshold for the initiation of spiral waves in active media.

[1] A. T. Winfree, *When Time Breaks Down* (Princeton University Press, Princeton, NJ, 1987).

[2] *Chemical Waves and Patterns*, edited by R. Kapral and K. Showalter (Kluwer, Dordrecht, 1995).

[3] I. R. Epstein and K. Showalter, J. Phys. Chem. **100**, 13132 (1996).

[4] M. C. Cross and P. C. Hohenberg, Rev. Mod. Phys. **65**, 851 (1993).

[5] M. Bär and M. Eiswirth, Phys. Rev. E **48**, R1635 (1993).

[6] Q. Ouyang, H. L. Swinney, and G. Li, Phys. Rev. Lett. **84**, 1047 (2000).

[7] K. Krischer and A. Mikhailov, Phys. Rev. Lett. **73**, 3165 (1994).

[8] S. Grill, V. S. Zykov, and S. C. Müller, Phys. Rev. Lett. **75**, 3368 (1995).

[9] V. K. Vanag, L. Yang, M. Dolnik, A. M. Zhabotinsky, and I. R. Epstein, Nature (London) **406**, 389 (2000).

[10] A. S. Mikhailov and V. S. Zykov, Physica D **52**, 379 (1991).

[11] A. N. Zaikin and A. M. Zhabotinsky, Nature (London) **225**, 535 (1970).

[12] L. Kuhnert, Nature (London) **319**, 393 (1986).

[13] I. Sendiña-Nadal, E. Mihaliuk, J. Wang, V. Pérez-Muñuzuri, and K. Showalter, Phys. Rev. Lett. **86**, 1646 (2001).

[14] R. J. Field and R. M. Noyes, J. Chem. Phys. **60**, 1877 (1973).

[15] J. J. Tyson and P. C. Fife, J. Chem. Phys. **73**, 2224 (1980).

[16] H.-J. Krug, L. Pohlmann, and L. Kuhnert, J. Phys. Chem. **94**, 4862 (1990).

[17] The coefficient D in Eq. (5) is equal to D_u in Eqs. (3) only in the case where the slow variable v is negligible in the dynamics of the front propagation. For a detailed discussion, see V. S. Zykov, Biophysics, (Engl. Trans.) **25**, 906 (1980).

[18] A. S. Mikhailov, *Foundations of Synergetics. I. Distributed Active Systems* (Springer-Verlag, Berlin, 1990).

[19] V. A. Davydov, V. S. Zykov, and A. S. Mikhailov, Sov. Phys. Usp. **34**, 665 (1991).

[20] E. Meron, Phys. Rep. **218**, 1 (1992).

[21] A. Karma, Phys. Rev. Lett. **66**, 2274 (1991).

[22] V. Hakim and A. Karma, Phys. Rev. E **60**, 5073 (1999).

[23] The dependence of area on the threshold value in Eq. (2) is slight for all but the smallest waves, but there is a significant dependence for these waves. This dependence gives rise to a quantitative shift in the curve shown in Fig. 3; however, the qualitative features remain unchanged.